C Journal of Carbon Research

MDPI

Article

Resistive Gas Sensors Based on Porous Sp-Containing Films Obtained by Dehydrohalogenation of PVDC and PVDC-PVC Copolymer

Oleg A. Streletskiy [1,*], Ilya A. Zavidovskiy [2,*], Islam F. Nuriahmetov [1], Olesya Y. Nishchak [1], Alexander V. Pavlikov [1] and Natalya F. Savchenko [1]

[1] Faculty of Physics, M.V. Lomonosov Moscow State University, Moscow 119991, Russia; islam.nuriakhmetov@mail.ru (I.F.N.); nischak@physics.msu.ru (O.Y.N.); pavlikov@physics.msu.ru (A.V.P.); n.f.savchenko@gmail.com (N.F.S.)

[2] Center for Photonics and 2D Materials, Moscow Institute of Physics and Technology, Dolgoprudny 141700, Russia

* Correspondence: streletskiy.oleg@gmail.com (O.A.S.); zavidovskii.ia@mipt.ru (I.A.Z.)

Abstract: Resistive sensing responses of the thin films obtained by dehydrohalogenation of polyvinylidene chloride (PVDC) and polyvinylidene chloride–polyvinyl chloride (PVDC-PVC) copolymer were investigated. The structure of the samples was studied by transmission electron microscopy, Fourier-transform infrared spectroscopy and Raman spectroscopy. The analyses demonstrate the formation of a porous structure based on polyyne–polyene chains. The formation of a foam-like oxidized sp-rich structure was observed for the samples obtained via the chemical treatment of the PVDC. However, a loose film with a developed structure and a lower fraction of sp-hybridized carbon was observed for KOH-treated PVDC-PVC. The resistive sensing responses of both of the dehydrohalogenated structures were measured for various concentrations of acetone, acetic acid, ammonia hydroxide, methanol, ethanol, benzene and water. The interplay between the efficiency of the dehydrohalogenation of the films, their structure and sensing selectivity is discussed.

Keywords: carbonization of linear polymers; foam-like sp-based coatings; selective sensing of acetic acid; polyyne–polyene structure

Citation: Streletskiy, O.A.; Zavidovskiy, I.A.; Nuriahmetov, I.F.; Nishchak, O.Y.; Pavlikov, A.V.; Savchenko, N.F. Resistive Gas Sensors Based on Porous Sp-Containing Films Obtained by Dehydrohalogenation of PVDC and PVDC-PVC Copolymer. *C* **2023**, *9*, 82. https://doi.org/10.3390/c9030082

Academic Editor: Dimitrios Kalderis

Received: 5 July 2023
Revised: 18 August 2023
Accepted: 26 August 2023
Published: 28 August 2023

1. Introduction

Development of reliable, reproducible, durable and selective gas sensing devices is a crucial task, as industrial facilities tend to rely on sensors allowing them to control toxic, flammable, explosive and harmful gases. Marketing research and quality control in pharmaceutical, fragrance and food industries also involve gas sensing, not to mention environmental monitoring. Various approaches, such as ion mobility spectroscopy and gas chromatography can be applied to investigate aerial environment [1]. Nevertheless, safety and quality control are usually associated with the detection of a limited amount of gases, which can be done by relatively simple devices measuring the variation of infrared absorption, electrochemical response, thermal conductivity, quartz crystal microbalance and electrical resistivity of the materials. Among these techniques, resistive gas sensing is of particular interest due to the low cost, high stability and sensitivity of the sensors [1]. Although the use of resistive sensors is hampered by their low selectivity and high operational temperature, chemically modified carbon materials are known to overcome these drawbacks [2]. In our previous work, we demonstrated that these disadvantages may be overcome by using dehydrofluorinated polyvinylidene fluoride (PVDF) as a sensing material [3]. As the modification of the material by dehydrohalogenation is known to induce the formation of pores and chemically active sites [4], such chemical treatment is a promising way to enhance the gas-sensing capabilities of the material. Dehydrohalogenation was previously used to form chemically active nitrile imines and nitrile oxides [5],

make partially dehydrofluorinated powder capable of energy storage [6] and neutralize toxic polychlorinated dibenzo-p-dioxin compounds [7]. However, the applicability of the dehydrohalogenation procedure to the formation of the functionalized continuous materials was hampered due to the limited interaction area between the chemically active solution and a precursor. The approach introduced in [3] allowed us to suggest a route which makes it possible to form a continuous structure with a modified surface layer by means of drop-casting of PVDF and its subsequent dehydrohalogenation.

Interestingly, the chemical treatment of PVDF led to the formation of sp-containing carbon (i.e., the material containing sp-hybridized carbon atoms). Such material is denoted as "polyyne–polyene" in our studies. Such notation indicates that the obtained material has a chain-like structure, which is comprised from both sp- (polyynic) and sp^2-hybridized (polyenic) linear fragments. In our previous studies, such structures were confirmed as a result of the dehydrohalogenation of PVDC [8] and PVDF [3]. Sp-containing materials are of recent interest, as theoretical studies reveal a tunable bandgap of such materials depending on the length of the carbon chain [9], their prominent thermal conductivity and mechanical strength [10]. Additionally, the effects of spin-polarized transport of electrons [11], strain-induced transition between metallic and insulator states [12] and ballistic conductivity [13] were predicted for sp-hybridized chains, thus making sp-containing materials highly promising for various applications related to their electrical performance. As PVDF sensing revealed that polyyne–polyenes have a high sensing selectivity to ammonia vapor [3], in the current paper, we investigate other linear polymers with structures akin to the one of PVDF, such as polyvinylidene chloride (PVDC) and polyvinylidene chloride–co-vinyl chloride (PVDC-PVC) copolymer. PVDC/PVC carbonization is considered to be more efficient in comparison to PVDF, as bonding energy of C-F is higher than the one of C-Cl [14,15]. Therefore, it was suggested that the formation of sp-hybridized carbon during PVC/PVDC dehydrohalogenation by potassium hydroxide treatment is more prominent than for PVDF.

Ammonia sensing is a crucial task, as ammonia, being the second-highest produced chemical commodity used in packaging, refrigerants, explosives, fertilizers and pharmaceuticals, is also an environmental contaminant and toxic substance [16]. Therefore, the disruptions of the technological processes involving ammonia pose a considerable threat to both human health and nature, and the development of novel, cheap and reliable methods of NH_3 concentration monitoring in ambient conditions is of considerable interest to industrial and scientific communities. As PVDF-devived material showed a prominent selective sensing of ammonium-containing vapor [3], the current study aimed to investigate if dehydrohalogenated PVDC and PVDC-PVC can also be the bases of NH_3-sensitive resistive sensors.

In the current paper, dehydrohalogenated PVDC and PVC/PVDC materials were investigated by transmission electron microscopy (TEM), Fourier-transform infrared spectroscopy (FTIR) and Raman spectroscopy, and their sensing response to acetone, ammonia hydroxide, ethanol, benzene and water vapors was assessed, allowing us to provide an insight into the sensing properties of the sp-containing structures.

2. Experimental Section

2.1. Formation of Polyyne–Polyenes and Sp-Based Sensors

The synthesis of polyyne–polyene coatings with resistive sensing capabilities was carried out via the drop-casting of the dissolved PVDC and PVDC-PVC and their subsequent carbonization in potassium hydroxide solution. Polyvinylidene chloride (PVDC) and polyvinylidene chloride–co-vinyl chloride (PVDC-PVC) powders (Aldrich Chemical Company, Inc., Milwaukee, WI, USA) were used as precursors. For the copolymer, the vinylidene chloride fraction was 65%, and the vinyl chloride fraction was 35%. Two types of samples based on those precursors were produced separately, but the procedure was similar.

A 5 mg dose of the polymer powder was dissolved at 70 °C in 10 mL of the mixture of acetone and N,N-dimethylformamide (DMF) in a 3:7 proportion. To implement conventional drop-casting, we poured the solution into Petri dishes, where it dried until the

evaporation of the liquid. In this stage, we synthesized semitranparent coatings of 100 nm thickness.

Afterwards, a carbonization of the drop-cast polymer films was implemented. First, KOH and CH_3OH solution was obtained by dissolving KOH powder. This solution was diluted by acetone in a 1:9 proportion. To initiate the carbonization, potassium hydroxide, methanol and acetone mixture was poured into the Petri dishes containing drop-cast PVDC and PVDC-PVC films.

PVDC and PVDC-PVC were carbonized by dehydrochlorination ensuring the removal of polymer side-groups. In Equation (1), we show a more general case of the reaction taking place for PVDC-PVC, where we assume n + m = p + q (adopted from [17]):

$$(\text{-}CH_2\text{-}CCl_2\text{-})_n \ldots (\text{-}CH_2\text{-}CHCl\text{-})_m + 2(n+m)KOH \rightarrow (\text{-}CH{=}CCl\text{-})_p \ldots (\text{-}C{\equiv}C\text{-})_q + 2(p+q)H_2O + 2(p+q)KCl \quad (1)$$

The formation of the chains consisting of sp-hybridized polyynic $(–C{\equiv}C–)_q$ and sp^2-hybridized polyenic $(–CH{=}CCl–)_p$ fragments leads to the synthesis of the polyyne–polyene sp-containing disordered material containing various side-groups and capping groups [3].

The carbonization lasted at ambient conditions for 24 h. During the dehydrohalogenation, the coatings separated from the surface of the Petri dishes, changing the appearance from translucent to opaque black.

Afterward, the residual products were removed from the synthesized material by cleaning in the ultrasonic cleaner (Wahluen electronic tools, Shantou, China) filled with distilled water for 15 min. Afterwards, that film was placed into acetone. Distilled water was purified on-site via the electric medical water distiller DE-4-02 (“EMO”, Saint-Petersburg, Russia). The thickness of the obtained material was 100 nm.

Aluminum films were deposited onto the carbonized coatings to manufacture the contacts of gas sensors (see Figure 1). To ensure the sensing area stayed uncoated, masks made of stainless steel were attached to the polyyne–polyene coatings. The masked samples were fixed on the substrate holder of the film deposition setup, then the 1.3×10^{-3} Pa residual pressure was achieved in the chamber via the turbomolecular pump. Afterwards, argon flow into the chamber was initiated, ensuring a working pressure of 1×10^{-2} Pa. In these conditions, aluminum films were deposited by radiofrequency (13.56 MHz) magnetron sputtering of an Al target at 100 W magnetron discharge power. Deposited contacts’ thickness was controlled by the quartz piezoelectric sensor.

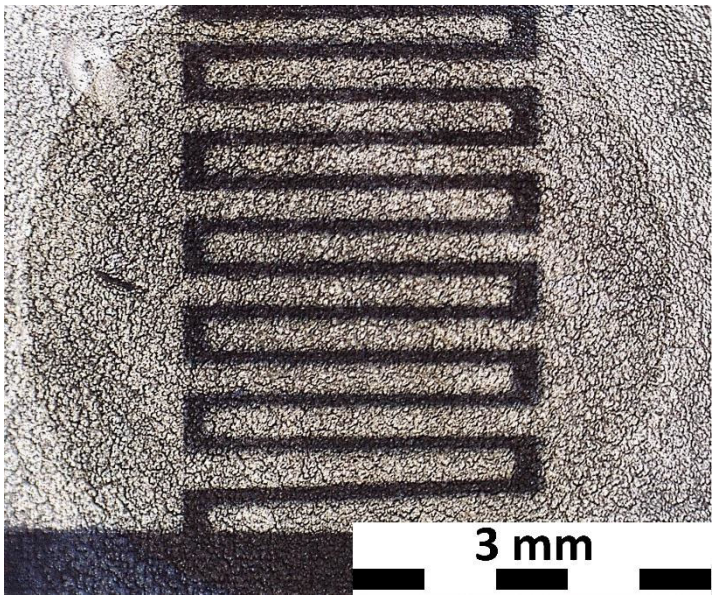

Figure 1. Polyyne–polyene-based sensor partially coated by aluminum. The length of the whole scale bar is 3 mm.

2.2. Characterization of the Samples' Structure

The transmission electron microscopy (TEM) was investigated by LEO 912 AB (Carl Zeiss, Jena, Germany). For TEM analyses, we used the structures produced from the ~100 nm thick PVDC and PVDC-PVC films. The synthesis conditions for these materials were the same as the ones of other samples. The energy of incident electrons was 120 keV. Grids used for the TEM studies consisted of copper cellular frames coated by thin polymer films. To place the structure onto TEM grids, samples were pressed to the polymer-coated side of the grids and removed after 5–10 s of grid-sample interaction. This technique was reported in [18].

Raman spectra were obtained via the Horiba HR 800 micro-Raman spectrometer. The excitation power was 1 mW, the wavelength was 488 nm and ×50 objective lens (N.A. = 0.85) was used. Spectra were measured from 3–5 regions of the films, and, after the comparison, the most typical spectra for each sample were chosen for the subsequent procession.

Brucker IFS-66v/S FTIR spectrometer (Bruker Optics, Karlsruhe, Germany) was used for Fourier-transform infrared spectroscopy (FTIR) investigation. The resolution of the Brucker IFS-66v/S spectrometer is 0.5 cm^{-1}.

2.3. Sensing Response Measurements

For the investigation of the room-temperature sensing response, polyyne–polyene films with aluminum contacts were placed inside the glove box (Plas Labs, Lansing, MI, USA), and their contacts were connected to the nanoamperemeter (Tektronix 4050, Beaverton, OR, USA). Equation (2) was used for the assessment of the relative sensing response $\Delta\sigma/\sigma_0$. In Equation (2), $\Delta\sigma$ is a sensing response, i.e., the difference of the conductivities in the sensing and non-sensing state, σ_{max} is the maximum conductivity of the sample measured throughout its interaction with the vapor, σ_0 is the conductivity of the sensor in the ambient atmosphere.

$$\Delta\sigma/\sigma_0 = (\sigma_{max} - \sigma_0)/\sigma_0 \quad (2)$$

The response and relaxation periods were estimated as times required for the conductivity change from σ_0 to $\sigma_0 + 0.9\Delta\sigma$ (response) and from σ_{max} to $\sigma_{max} - 0.9\Delta\sigma$ (relaxation). The experiments were carried out 3–4 times for each sample and gas.

3. Results

3.1. TEM

Figure 2a,b shows the TEM images of the sp-containing film derived from PVDC. Hereinafter, dehydrohalogenated PVDC and PVDC-PVC structures are defined as dh-PVDC and dh-PVDC-PVC, respectively. TEM analysis of dh-PVDC shows that its structure resembles foam. Its pores of 60 nm diameter are separated by fragments of the material of ~5–15 nm width and ~1 nm thickness. This morphology is formed due to the high efficiency of the dehydrochlorination leading to chlorine substitution, leading to potassium chlorine formation. This process induces the shrinkage of the material due to the mass reduction.

As for the chemically treated PVDC-PVC, a loose film with a developed structure was observed. The development of the dh-PVDC is unsurprisingly more prominent than that of the dh-PVDC-PVC, as PVDC-PVC contains a larger fraction of hydrogen, and C-H bonds have larger dissociation energy than C-Cl [19,20]. Although the vinyl chloride proportion in the PVDC-PVC material is only 35%, significant variation between the morphology of the samples derived from dh-PVDC and dh-PVDC-PVC is observed.

3.2. Raman Spectroscopy

Typical Raman spectra of dh-PVDC and dh-PVDC-PVC are shown in Figure 3. The subtraction of the spectra background was carried out by OriginPro software. After the background subtraction, the spectra were normalized to similar intensity and, for better distinguishment, a horizontal slope was applied to the spectrum derived from PVDC-PVC.

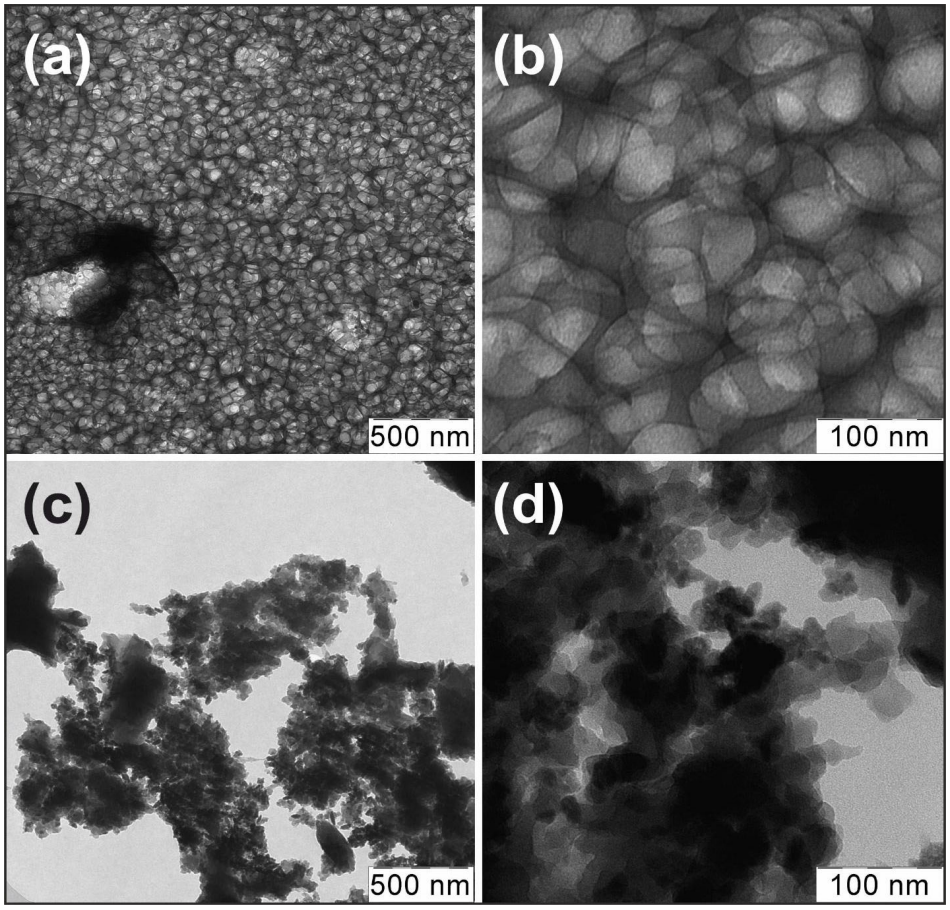

Figure 2. TEM images of (**a**,**b**) dehydrochlorinated PVDC, (**c**,**d**) dehydrochlorinated PVDC-PVC.

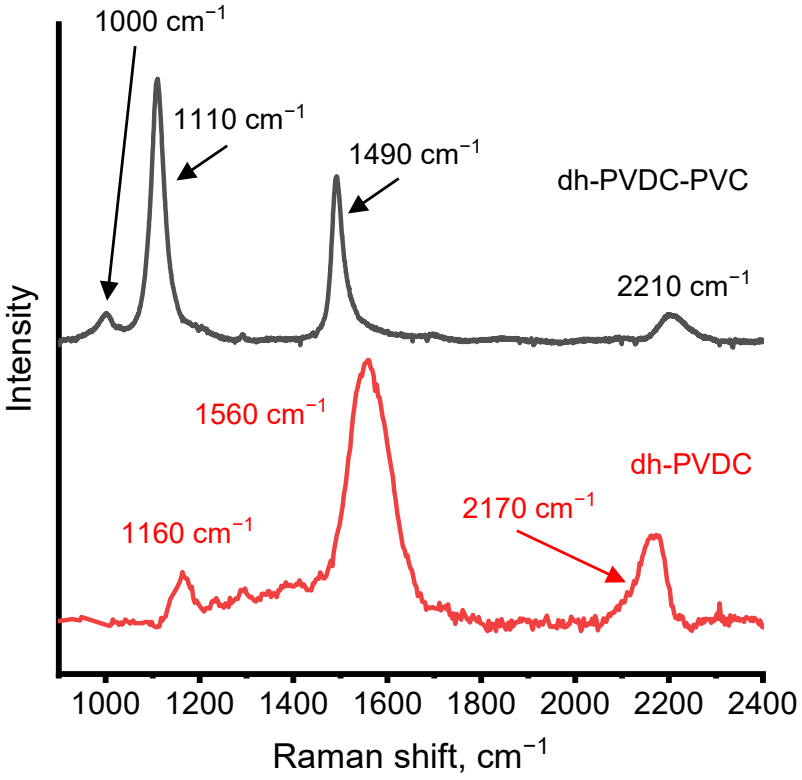

Figure 3. Raman spectra of the sp-containing films derived from PVDC (red line) and PVDC-PVC (black line). The positions of the lines whose origin is discussed in the text are indicated.

The spectrum of dh-PVDC (red line in Figure 3) shows relatively wide lines at 1160, 1560 and 2170 cm^{-1}. These lines are related to the vibrations of the C-C and of trans-isomeric polyenic structures [21], C=C of various carbon-based materials including disordered carbon and polyenes [8], and the vibrations of C≡C bonds [22–24], respectively. The plateau at 1210–1460 cm^{-1} is mainly attributed to the contribution of the D-line related to the breathing mode of sp^2-hybridized clusters [25]. Its emergence is generally related to the disorder of the sp^2-hybridized component. The fitting of the similar spectra and its more detailed discussion are presented in [8].

As for the spectrum of dh-PVDC-PVC (black line in Figure 3), it shows relatively narrow lines. The positions of the polyene-related C-C and C=C bands of the dh-PVDC-PVC material are shifted to the lower wavenumbers of 1110 cm^{-1} for C-C and 1490 cm^{-1} for C=C, indicating that the sp^2-carbon fragments of the dh-PVDC-PVC structure are longer than that of dh-PVDC [26,27]. The line centered at 1000 cm^{-1} is ascribed to the out-of-plane wagging of C-H typical for the Raman response of distorted polyenes [28]. As for the Raman line centered at 2210 cm^{-1}, it is centered close to the position of the doubled 1100 cm^{-1}; therefore, we assign it to the second order of C-C-related peak [28]. Although vibrations of the C≡C bonds may contribute to the Raman spectra in the 1800–2240 cm^{-1} region [29], we assume the polyyne contribution to the observed line in the studied case to be small.

The analysis of the Raman spectra shows that the formation of $(-C{\equiv}C-)_n$ polyynic fragments is more prominent for dehydrochlorinated PVDC than for dehydrochlorinated PVDC-PVC copolymer; however, a more prominent dehydrohalogenation of PVDC apparently results in a more distorted highly porous sp-containing structure. The dh-PVDC-PVC film shows a more ordered polyenic structure with only a slight fraction of sp-carbon fragments.

3.3. FTIR

FTIR spectra of the materials obtained by PVDC and PVDC-PVC dehydrohalogenation are shown in Figure 4. The set of lines at 440–460, 590–600 and 650–660 cm^{-1} is typical for the stretching of C-Cl_2 bonds [30]. Chlorine presence may be caused by partial dehydrochlorination of the structure, as the interaction of the KOH and deep layers of polymers is suppressed. The band positioned at 530–540 cm^{-1} is attributed to the skeletal vibrations of the PVDC backbone. It emerges for the dh-PVDC only, and its intensity is even higher than that of an untreated PVDC [8,30], whose presence indicates the possibility of the elongation of the chains during their cross-linking, which may be induced by the removal of their capping groups. For the dh-PVDC-PVC, this line cannot be observed, apparently due to the insufficient length of PVDC fragments for this line to be infrared-active. The lines at 740–750 cm^{-1} and 870–880 cm^{-1} are ascribed to CH_2 [30].

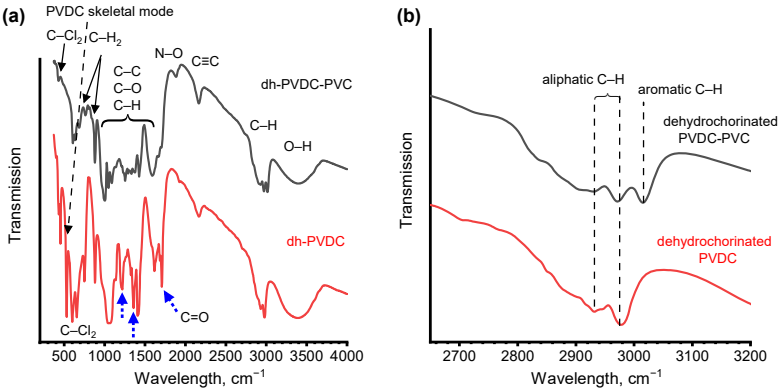

Figure 4. (**a**) FTIR spectrum of sp-containing films obtained by the dehydrochlorination of PVDC-PVC and PVDC. Chemical bonds attributed to various bands are indicated. Blue arrows indicate the bands attributed to carbon–oxygen bonding. (**b**) FTIR spectrum of sp-containing films in the region related to C-H bonds.

The wide bands positioned in the range of 900–1600 cm^{-1} are typical for carbon components, and their assignment is not as straightforward as that of the bands attributed to PVDC. The bands at 1010–1070 and 1200–1260 cm^{-1} are assigned to C-C, C-O-C and C-O [3,31,32]. The band at 1350–1360 cm^{-1} is assigned to C-H and C-O [31,33]. The band at 1400–1430 cm^{-1} can be attributed to C-O and C-H_x [34–36]. The line located at 1600–1630 cm^{-1} is assigned to C=C [23]. In the chained structures, the FTIR activity of the bands associated with C-C and C=C may be caused by the presence of imperfections in the chains, such as a deformation of their structure and the presence of side- and end-groups.

The intensive band positioned at 1710 cm^{-1} is assigned to C=O [31]. Notably, the lines located at 1200–1260, 1350–1360 and ~1710 cm^{-1} are more intensive for the PVDC-derived material, and all of them are, at least partially, attributed to C-O and C=O bonding. These oxygen-related lines of dh-PVDC are indicated by blue arrows in 4(a). In its turn, the line at 1880–1940 cm^{-1} may be related to N-O [37,38] of the surface adsorbates and contaminations.

The band positioned at 2160–2170 cm^{-1} is ascribed to C≡C bonding [22–24]. It is active both in FTIR and in Raman spectra, which is caused by the violation of the exclusion principle taking place for long bended chains [39]. Notably, the position of the peak shows that sp-hybridized fragments have a single C≡C bond [40].

C-H-related lines of dh-PVDC are located at 2930 and 2970 cm^{-1}, as shown in Figure 4b. These locations are typical for aliphatic (i.e., non-aromatic) hydrocarbon fragments [41,42], which proves that hydrocarbons comprising the structure are predominantly non-aromatic, which corroborates its chain-like structure. In its turn, the dh-PVDC-PVC shows not only lines related to aliphatic carbon structure at 2930 and 2970 cm^{-1} but also the 3020-cm^{-1}-centered line, which is related to the vibration of aromatic carbon bonded to hydrogen [43]. The wide line at 3060–3700 cm^{-1} is related to the O-H vibrations of adsorbed water [44].

Thus, the materials obtained from both of the precursors show the presence of sp/sp^2-hybridized carbon, predominantly existing in the chained form, and non-treated polymeric fragments. The differences in the FTIR and the Raman spectra can be summarized as follows: the film obtained by PVDC dehydrochlorination is more disordered, oxidized and, according to the Raman analysis, features a larger fraction of sp-carbon. At the same time, the dh-PVDC-PVC sample shows a more prominent presence of the ordered, yet distorted, polyenes and aromatic carbon. These results corroborate the TEM studies indicating the higher effectiveness of the dehydrohalogenation process of the PVDC sample, thus resulting in a more prominent formation of a porous structure with the dangling bonds subsequently saturated by atmospheric oxygen. At the same time, more fragments of the dh-PVDC-PVC are dehydrohalogenated incompletely, because hydrogen elimination from the polymer by KOH is less effective compared to that of chlorine. As a result, the PVDC-PVC chemical rearrangement leads tothe formation of sp^2-hybridized polyenic and phenylic clusters passivated by hydrogen rather than $(-C\equiv C-)_n$ polyyne fragments. The oxidation of dehydrohalogenated PVDC-PVC may be suppressed not only by a lower fraction of dangling bonds, due to the relatively low porosity of the resulting structure.

3.4. Sensing Properties

In Figure 5, the variation of $\Delta\sigma/\sigma_0$ at different gas concentrations is presnted. The saturation at large concentrations of analyzed vapors is characteristic for the Langmuir adsorption isotherm [45]. For the dh-PVDC, a prominent decrease in the slope of $\Delta\sigma/\sigma_0$ dependence of ethanol, methanol, acetone and water was observed. However, it was not observed for $\Delta\sigma/\sigma_0$ dependence on the concentration of ammonium hydroxide and acetic acid; for these gases, saturation can apparently be observed at larger concentrations of vapors. For dh-PVDC-PVC in the present range of concentrations, saturation was observed for all types of gases. Notably, the resistive response on benzene and acetone, in the case of dh-PVDC-PVC material, was observed only at the range of concentrations exceeding 15×10^3 ppm. In the case of the dh-PVDC, the resistive response on benzene was not

observed, but for acetone, the resistive response was observed only after 15×10^3 ppm. The saturation is observed for all types of gases, which suggests that charge carrier transfer between vapor molecules and sensing material is governed by similar mechanisms.

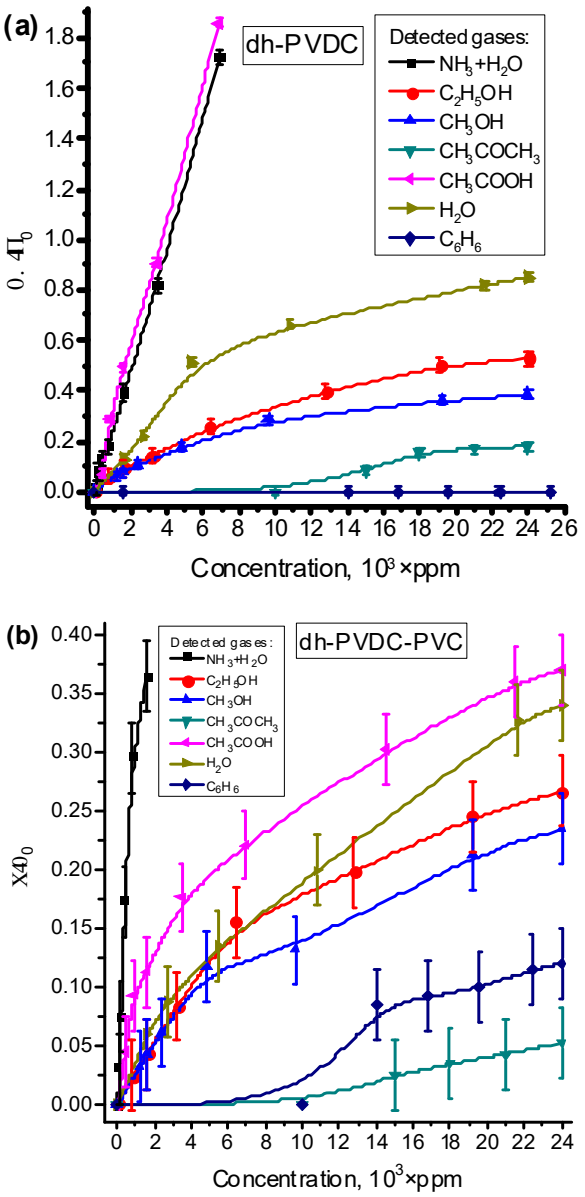

Figure 5. Normalized resistive sensing response of the polyene–polyyne structure based on PVDC (**a**) and PVDC-PVC (**b**) precursors to various concentrations of vapors.

For both analyzed structures, electrical conductance enlarges after the vapor absorption. The origin of such a response is an electron transfer between adsorbed gas and the highest occupied molecular orbital (HOMO) or the lowest unoccupied molecular orbital (LUMO) of the material. Methanol CH_3OH, ethanol C_2H_5OH, ammonium NH_3, ammonium hydroxide NH_3+H_2O and water H_2O act as electron donors when they are adsorbed by polymers [46,47] and carbon materials such as nanotubes [48], graphene [49] and porous carbon [50]. As electron transfer from adsorbed gas HOMO to the LUMO of the material leads to an increase in its electrical conductivity; the observed response to all gases confirms that the structure is an n-type semiconductor. Ammonium is a most prominent example of the electron donor gas, and polymeric materials typically have prominent resistive sensing responses to NH_3 due to the efficiency of the mechanism discussed above [51]. In the

current study, ammonium hydroxide was chosen as the ammonium source which made it possible to determine the materials' response to NH_3 vapor.

The study of time-dependent sensing response was carried out for the acetone, ammonia hydroxide, ethanol, benzene, acetic acid and water vapors of 1.6×10^3 ppm concentrations. In the case of acetic acid sensing, the response and the relaxation periods for the dh-PVDC were 260 and 360 s, and for the dh-PVDC-PVC both the response and the relaxation occurred for 200 s (see Figure S1). When the acetic acid was introduced into the chamber, the resistivity of the dh-PVDC sensing film began to increase. As shown by the structural investigation (Section 3.3), oxygen passivation forms on the surface of the sample under exposure to ambient atmosphere. As shown in [52,53], in the absence of the detected gas, oxygen-containing, functional groups capture and trap electrons from the conduction band of the material. In their turn, when the structure is exposed to gaseous CH_3COOH, gas molecules of acetic acid interact with the adsorbed oxygen on the sample surface. As a result of the interaction between the gas molecules with the absorbed oxygen, acetic acid molecules are oxidized and the electrons are released back into the conduction band of the material [54]. As shown in [3], polyyne–polyene material is an n-type semiconductor; therefore, its conductivity increases after the acetic acid exposure leading to the electrons detrapping. This effect is to some extent unconventional, as CH_3COOH is a prominent electron-withdrawing gas [55], therefore its interaction with non-oxidized n-type polymers typically leads to resistivity increase.

PVDC-PVC-derived material shows a sensing response to acetic acid which is 4.4 times larger compared to that of the dh-PVDC samples, which is apparently related to its higher oxygenation, which leads to the prominent effect of the electron detrapping after CH_3COOH and dh-PVDC interaction.

In the case of ammonium hydroxide sensing, the response and the relaxation periods are: for the dh-PVDC—75 and 190 s, and the dh-PVDC-PVC—430 and 550 s (see Figure S1). Such a considerable difference can be explained by slower adsorption between dh-PVDC-PVC and ammonia molecules caused by a strong bonding between the analyte and the material. However, the intensities of the sensing response to ammonium hydroxide for both of the structures are almost equal.

Notably, the sensing response of dh-PVDC to the gases other than ammonium hydroxide is significantly larger compared to that of dh-PVDC-PVC, which can be attributed to a more developed foam-like structure of dh-PVDC. A larger fraction of highly reactive sp-carbon fragments in dh-PVDC can also increase its chemosensing aptitude. However, previously we concluded that in polyyne–polyene structures the sp-carbon effect on the resistive sensing response is only slight, as the levels in the band structure related to the π-electrons of sp-hybridized carbon only slightly affect the electronic properties of polymeric materials [3]. Thus, the similarity of the dh-PVDC and the dh-PVDC-PVC to sensing response to ammonium is apparently caused by a more potent interaction between dh-PVDC-PVC and HN_3 and a more developed structure of dh-PVDC.

Figure 6 shows a comparison of the sensing responses of the samples to different gases. For the dh-PVDC sample, the ratios of the responses to various vapors are $\Delta\sigma_{NH_3+H_2O}/\Delta_{C_2H_5OH} = 4.4$, $\Delta\sigma_{NH_3+H_2O}/\Delta\sigma_{CH_3OH} = 4.9$, $\Delta\sigma_{NH_3+H_2O}/\Delta\sigma_{CH_3COOH} = 0.8$ and $\Delta\sigma_{NH_3+H_2O}/\Delta\sigma_{H_2O} = 3$. For the PVDC-PVC sample, the ratios of the responses to various vapors are $\Delta\sigma_{NH_3+H_2O}/\Delta\sigma_{C_2H_5OH} = 8.5$, $\Delta\sigma_{NH_3+H_2O}/\Delta\sigma_{CH_3OH} = 8.7$, $\Delta\sigma_{NH_3+H_2O}/\Delta\sigma_{CH_3COOH} = 3.2$ and $\Delta\sigma_{NH_3+H_2O}/\Delta\sigma_{H_2O} = 6.1$.

It is worth noticing that the selectivity of the sensing response of the studied polyyne–polyene materials to ammonia is significantly less than that of similar materials obtained by dehydrofluorination of polyvinylidene difluoride (dh-PVDF) reported in [3]. $\Delta\sigma_{NH_3+H_2O}/\Delta\sigma_{C_2H_5OH}$ of dh-PVDF is 74 times higher than that of dh-PVDC, while $\Delta\sigma_{NH_3+H_2O}/\Delta\sigma_{H_2O}$ of dh-PVDF is 26 times higher [3]. Such a prominent change can be attributed to the presence of residual polyvinylidene difluoride (PVDF) fragments in dh-PVDF. The selective PVDF response to ammonia has been reported for polyani-

line/polyvinylidene difluoride composites [56,57]; however, PVDF's role in the sensing of polymer-based nanocomposites requires further investigation.

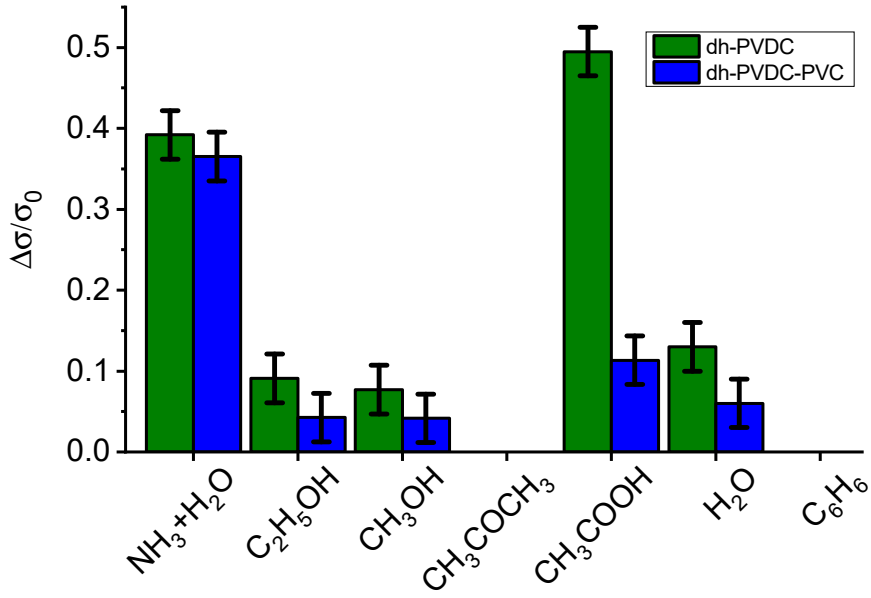

Figure 6. Comparison of the sensing responses of the samples to different gases.

In summary, according to our studies, the sensing response mechanism of the dh-PVDC and dh-PVDC-PVC can be explained by the doping of the structures caused either by the chemical interaction between the vapor molecules and the surface of polyyne–polyene material, or by the electron transfer between the molecule and the sensing structure. The latter mechanism is prevalent for the gases with prominent electron donor capabilities, such as ammonia, which strongly interact with both dh-PVDC and dh-PVDC-PVC structures (Figure 7a). In its term, considerable chemical interaction takes place between the acetic acid and dh-PVDC; although CH_3COOH is a prominent electron acceptor, its interaction with the oxidized surface results in electron detrapping and also leads to the conductivity increase (Figure 7b). Other analyzed vapors act as weak electron donors during the interaction with the polyyne–polyene surface, and their response results only in a slight increase in the samples' conductivity (Figure 7c). As surface chemistry was found to play a significant role in the sensing response, subsequent studies should be aimed at a more detailed analysis of polyyne–polyenes' oxidation, chemical stability and longevity of their performance.

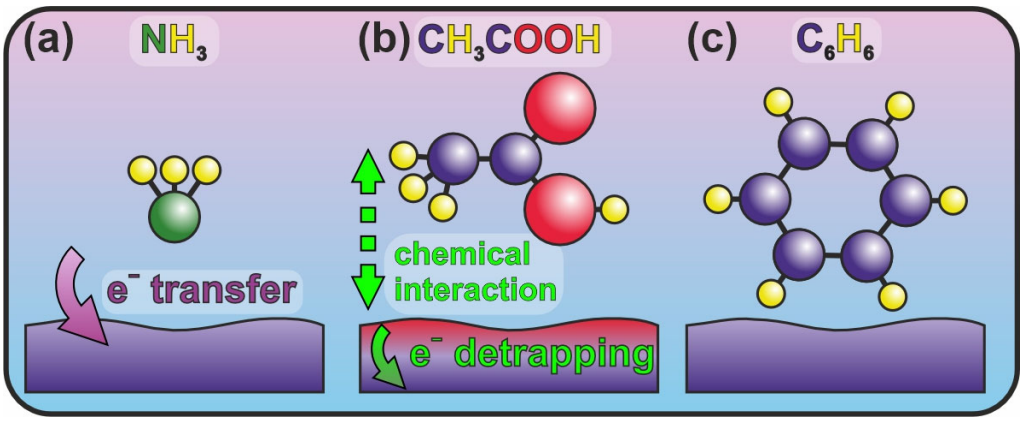

Figure 7. Illustration of the sensing mechanism of the investigated structures: (**a**) To prominent electron donors; (**b**) To CH_3COOH interacting with oxygen-rich surface of dh-PVDC; (**c**) To other gases not possessing electron donor capability.

4. Conclusions

In this paper, sp-containing films of a polyyne–polyene structure prepared by PVDC-PVC and PVC drop-casting and subsequent dehydrohalogenation were investigated. The porous dh-PVDC-PVC sample shows a prominent presence of polyenes and aromatic carbon. The foam-like coating containing 60-nm-sized pores obtained by PVDC dehydrochlorination (dh-PVDC) is more disordered and oxidized, featuring a larger fraction of sp-carbon. Both the more developed structure of the dh-PVDC and its more notable oxygenation and sp-carbon formation are explained by more efficient dehydrohalogenation of the PVDC structure containing less hydrogen than the PVDC-PVC.

Both the dh-PVDC-based and the dh-PVDC-PVC-based resistive gas sensors demonstrate a slightly selective response to ammonium hydroxide vapor due to the strong electron donor capability of ammonia. In turn, the dh-PVDC-based sensors also show a significant response to acetic acid vapor, which is explained by the effective interaction of CH_3COOH with the oxygenated material.

Surface functionalization [58,59] and metal doping [60] are typically associated with the improvement of the performance of the carbon-based sensors. Therefore, subsequent studies of polyyne–polyenes' sensing capabilities can be aimed at the formation of the carbon–metal hybrids or structures with modified surface layer, which are to be tailored towards selective ammonia sensing. However, as PVDF-derived material showed considerably higher NH_3 selectivity than dh-PVDC and dh-PVDC-PVC, we consider that subsequent development will be associated with dehydrofluorinated PVDF rather than PVDC/PVC.

Supplementary Materials: The following supporting information can be downloaded at: https://www.mdpi.com/article/10.3390/c9030082/s1, Figure S1: time-resolved relative resistive sensing response of dh-PVDC-PVC and dh-PVDC to ammonium hydroxide and acetic acid vapors.

Author Contributions: Conceptualization, O.A.S.; Data curation, O.A.S. and I.A.Z.; Formal analysis, O.A.S., I.A.Z. and I.F.N.; Funding acquisition, I.A.Z.; Investigation, O.A.S., I.F.N., O.Y.N. and A.V.P.; Methodology, O.A.S. and O.Y.N.; Project administration, O.A.S.; Resources, O.A.S.; Software, I.A.Z. and I.F.N.; Supervision, O.A.S. and A.V.P.; Validation, I.A.Z.; Visualization, O.A.S. and I.A.Z.; Writing—original draft, O.A.S., I.A.Z. and I.F.N.; Writing—review and editing, O.Y.N., A.V.P. and N.F.S. All authors have read and agreed to the published version of the manuscript.

Funding: I.A. Zavidovskiy gratefully acknowledges financial support from the Ministry of Science and Higher Education of the Russian Federation (No. 0714-2020-0002). This work was supported by the Ministry of Science and Higher Education of the Russian Federation (Agreement No. 075-15-2022-1150).

Data Availability Statement: Not applicable.

Conflicts of Interest: The authors declare no conflict of interest.

References

1. Wang, Z.; Zhu, L.; Sun, S.; Wang, J.; Yan, W. One-Dimensional Nanomaterials in Resistive Gas Sensor: From Material Design to Application. *Chemosensors* **2021**, *9*, 198. [CrossRef]
2. Musayeva, N.; Khalilova, H.; Izzatov, B.; Trevisi, G.; Ahmadova, S.; Alizada, M. Highly Selective Detection of Hydrogen Sulfide by Simple Cu-CNTs Nanocomposites. *C* **2023**, *9*, 25. [CrossRef]
3. Zavidovskiy, I.A.; Streletskiy, O.A.; Nuriahmetov, I.F.; Nishchak, O.Y.; Savchenko, N.F.; Tatarintsev, A.A.; Pavlikov, A.V. Highly Selective Polyene-Polyyne Resistive Gas Sensors: Response Tuning by Low-Energy Ion Irradiation. *J. Compos. Sci.* **2023**, *7*, 156. [CrossRef]
4. Giannakoudakis, D.A.; Bandosz, T.J. Defectous UiO-66 MOF Nanocomposites as Reactive Media of Superior Protection against Toxic Vapors. *ACS Appl. Mater. Interfaces* **2020**, *12*, 14678–14689. [CrossRef]
5. Shybanov, D.E.; Filkina, M.E.; Kukushkin, M.E.; Grishin, Y.K.; Roznyatovsky, V.A.; Zyk, N.V.; Beloglazkina, E.K. Diffusion Mixing with a Volatile Tertiary Amine as a Very Efficient Technique for 1,3-Dipolar Cycloaddition Reactions Proceeding via Dehydrohalogenation of Stable Precursors of Reactive Dipoles. *New J. Chem.* **2022**, *46*, 18575–18586. [CrossRef]
6. Qu, P.; Liu, X.; Wang, S.; Xiao, C.; Liu, S. Moderate Dehydrofluorinated PVDF with High Energy Density. *Mater. Lett.* **2018**, *221*, 275–278. [CrossRef]

7. González, S.; Porras, M.; Jimbo, A.; Zambrano, C.H. Dehydrochlorination of PCDDs on SWCN-Supported Ni10 and Ni13 Clusters, a DFT Study. *Molecules* **2022**, *27*, 5074. [CrossRef]
8. Streletskiy, O.A.; Zavidovskiy, I.A.; Nuriahmetov, I.F.; Khaidarov, A.A.; Pavlikov, A.V.; Minnebaev, K.F. The Field-Effect Transistor Based on a Polyyne–Polyene Structure Obtained via PVDC Dehydrochlorination. *J. Compos. Sci.* **2023**, *7*, 264. [CrossRef]
9. Pan, B.; Xiao, J.; Li, J.; Liu, P.; Wang, C.; Yang, G. Carbyne with Finite Length: The One-Dimensional Sp Carbon. *Sci. Adv.* **2015**, *1*, e1500857. [CrossRef]
10. Eaton, A.L.; Fielder, M.; Nair, A.K. Mechanical and Thermal Properties of Carbon-Based Low-Dimensional Materials. *MRS Bull.* **2022**, *47*, 1001–1010. [CrossRef]
11. Zanolli, Z.; Onida, G.; Charlier, J.-C. Quantum Spin Transport in Carbon Chains. *ACS Nano* **2010**, *4*, 5174–5180. [CrossRef]
12. La Torre, A.; Botello-Mendez, A.; Baaziz, W.; Charlier, J.-C.; Banhart, F. Strain-Induced Metal–Semiconductor Transition Observed in Atomic Carbon Chains. *Nat. Commun.* **2015**, *6*, 6636. [CrossRef]
13. Wang, M.; Lin, S. Ballistic Thermal Transport in Carbyne and Cumulene with Micron-Scale Spectral Acoustic Phonon Mean Free Path. *Sci. Rep.* **2015**, *5*, 18122. [CrossRef]
14. Hukka, T.I.; Pakkanen, T.A.; D'Evelyn, M.P. Chemisorption of Fluorine, Chlorine, HF, and HCl on the Diamond (100)2x1 Surface: An Ab Initio Study. *J. Phys. Chem.* **1995**, *99*, 4710–4719. [CrossRef]
15. Xu, B.; Hou, S.; Chu, M.; Cao, G.; Yang, Y. An Activation-Free Method for Preparing Microporous Carbon by the Pyrolysis of Poly(Vinylidene Fluoride). *Carbon* **2010**, *48*, 2812–2814. [CrossRef]
16. Chaudhary, V.; Gautam, A.; Mishra, Y.K.; Kaushik, A. Emerging MXene–Polymer Hybrid Nanocomposites for High-Performance Ammonia Sensing and Monitoring. *Nanomaterials* **2021**, *11*, 2496. [CrossRef]
17. Evsyukov, S.E. Chemical Dehydrohalogenation of Polymers. In *Carbyne and Carbynoid Structures*; Heimann, R.B., Evsyukov, S.E., Kavan, L., Eds.; Physics and Chemistry of Materials with Low-Dimensional Structures; Springer: Dordrecht, The Netherlands, 1999; Volume 21, pp. 55–74. ISBN 978-94-010-5993-0.
18. Streletskiy, O.; Zavidovskiy, I.; Yakubovsky, D.; Doroshina, N.; Syuy, A.; Lebedinskij, Y.; Markeev, A.; Arsenin, A.; Volkov, V.; Novikov, S. Tailoring of the Distribution of SERS-Active Silver Nanoparticles by Post-Deposition Low-Energy Ion Beam Irradiation. *Materials* **2022**, *15*, 7721. [CrossRef]
19. McGivern, W.S.; Derecskei-Kovacs, A.; North, S.W.; Francisco, J.S. Computationally Efficient Methodology to Calculate C−H and C−X (X = F, Cl, and Br) Bond Dissociation Energies in Haloalkanes. *J. Phys. Chem. A* **2000**, *104*, 436–442. [CrossRef]
20. Cioslowski, J.; Liu, G.; Moncrieff, D. Energetics of the Homolytic C−H and C−Cl Bond Cleavages in Polychlorobenzenes: The Role of Electronic and Steric Effects. *J. Phys. Chem. A* **1997**, *101*, 957–960. [CrossRef]
21. Abdu, Y.A. Raman Micro-Spectroscopy of Nanodiamonds from the Kapoeta Meteorite. *Diam. Relat. Mater.* **2021**, *118*, 108536. [CrossRef]
22. Zhivulin, V.E.; Khairanov, R.K.; Zlobina, N.A.; Pesin, L.A. Modification of the IR Spectra Shape in the 2000–2300 Cm–1 Absorption Band upon the Aging of a Chemically Dehydrofluorinated Poly(Vinylidene Fluoride) Film. *J. Surf. Investig.* **2020**, *14*, 1144–1151. [CrossRef]
23. Streletskiy, O.A.; Nishchak, O.Y.; Zavidovskiy, I.A.; Maslakov, K.I.; Pavlikov, A.V. Sp-Based Thin Films Synthesized by Magnetron Sputtering of Dehydrohalogenated Polyvinylidenchloride. *Thin Solid Film.* **2021**, *739*, 138993. [CrossRef]
24. Streletskiy, O.A.; Zavidovskiy, I.A.; Nishchak, O.Y.; Khaidarov, A.A.; Savchenko, N.F.; Pavlikov, A.V. Low-Threshold Field Emission Cathode Based on Heat-Treated Dehydrofluorinated Polyvinylidene Fluoride. *J. Exp. Theor. Phys.* **2022**, *135*, 844–852. [CrossRef]
25. Streletskiy, O.A.; Zavidovskiy, I.A.; Balabanyan, V.Y.; Tsiskarashvili, A.V. Antibacterial Properties of Modified A-C and Ta-C Coatings: The Effects of the Sp2/Sp3 Ratio, Oxidation, Nitridation, and Silver Incorporation. *Appl. Phys. A* **2022**, *128*, 929. [CrossRef]
26. Novikov, V.S.; Kuzmin, V.V.; Kuznetsov, S.M.; Darvin, M.E.; Lademann, J.; Sagitova, E.A.; Ustynyuk, L.Y.; Prokhorov, K.A.; Nikolaeva, G.Y. DFT Study of Raman Spectra of Polyenes and SS-Carotene: Dependence on Length of Polyene Chain and Isomer Type. *Spectrochim. Acta Part A Mol. Biomol. Spectrosc.* **2021**, *255*, 119668. [CrossRef] [PubMed]
27. Oshiro, T.; Yamazato, M.; Higa, A.; Toguchi, M. Raman Analysis of *Trans* -Polyacetylene Chains in Hydrogenated Amorphous Carbon Films. *Jpn. J. Appl. Phys.* **2007**, *46*, 756–760. [CrossRef]
28. Brambilla, L.; Tommasini, M.; Zerbi, G.; Stradi, R. Raman Spectroscopy of Polyconjugated Molecules with Electronic and Mechanical Confinement: The Spectrum of *Corallium Rubrum*: Raman Spectroscopy of Polyconjugated Molecules with Electronic and Mechanical Confinement. *J. Raman Spectrosc.* **2012**, *43*, 1449–1458. [CrossRef]
29. Buntov, E.A.; Zatsepin, A.F.; Guseva, M.B.; Ponosov, Y.S. 2D-Ordered Kinked Carbyne Chains: DFT Modeling and Raman Characterization. *Carbon* **2017**, *117*, 271–278. [CrossRef]
30. Coleman, M.M.; Wu, M.S.; Harrison, I.R.; Painter, P.C. Vibrational Spectra and Conformation of Poly(Vinylidene Chloride). *J. Macromol. Sci. Part B* **1978**, *15*, 463–480. [CrossRef]
31. Ţucureanu, V.; Matei, A.; Avram, A.M. FTIR Spectroscopy for Carbon Family Study. *Crit. Rev. Anal. Chem.* **2016**, *46*, 502–520. [CrossRef]
32. Pamuła, E.; Błażewicz, M.; Paluszkiewicz, C.; Dobrzyński, P. FTIR Study of Degradation Products of Aliphatic Polyesters–Carbon Fibres Composites. *J. Mol. Struct.* **2001**, *596*, 69–75. [CrossRef]

33. Burket, C.L.; Rajagopalan, R.; Marencic, A.P.; Dronvajjala, K.; Foley, H.C. Genesis of Porosity in Polyfurfuryl Alcohol Derived Nanoporous Carbon. *Carbon* **2006**, *44*, 2957–2963. [CrossRef]
34. Karimov, O.K.; Teptereva, G.A.; Chetvertneva, I.A.; Movsumzade, E.M.; Karimov, E.K. The Structure of Lignosulfonates for Production of Carbon Catalyst Support. *IOP Conf. Ser. Earth Environ. Sci.* **2021**, *839*, 022086. [CrossRef]
35. Venkatesh, R.; Karthi, N.; Kawin, N.; Prakash, T.; Kannan, C.R.; Karthigairajan, M.; Bobe, K. Synthesis and Adsorbent Performance of Modified Biochar with Ag/MgO Nanocomposites for Heat Storage Application. *Adsorpt. Sci. Technol.* **2022**, *2022*, e7423102. [CrossRef]
36. Kaur, G.A.; Sharma, V.; Gupta, N.; Shandilya, M.; Rai, R. Structural and Optical Amendment of PVDF into CQDs through High Temperature Calcination Process. *Mater. Lett.* **2021**, *304*, 130616. [CrossRef]
37. Hadjiivanov, K.; Concepción, P.; Knözinger, H. Analysis of Oxidation States of Vanadium in Vanadia–Titania Catalysts by the IR Spectra of Adsorbed NO. *Top. Catal.* **2000**, *11*, 123–130. [CrossRef]
38. Neto, E.L.d.O.; Cezar, J.G.; Doro, F.G.; Carvalho, J.R.M.; Ferreira, K.Q. Synthesis, Characterization and Reactivity of Nitrosyl Ruthenium Complexes with the Non-Stereoidal Anti-Inflammatory Diflunisal. *J. Chem. Environ. Biol. Eng.* **2020**, *4*, 39. [CrossRef]
39. Lucotti, A.; Tommasini, M.; Fazzi, D.; Del Zoppo, M.; Chalifoux, W.A.; Ferguson, M.J.; Zerbi, G.; Tykwinski, R.R. Evidence for Solution-State Nonlinearity of Sp-Carbon Chains Based on IR and Raman Spectroscopy: Violation of Mutual Exclusion. *J. Am. Chem. Soc.* **2009**, *131*, 4239–4244. [CrossRef]
40. Leong, T.X.; Collins, B.K.; Dey Baksi, S.; Mackin, R.T.; Sribnyi, A.; Burin, A.L.; Gladysz, J.A.; Rubtsov, I.V. Tracking Energy Transfer across a Platinum Center. *J. Phys. Chem. A* **2022**, *126*, 4915–4930. [CrossRef]
41. Begni, F.; Paul, G.; Lasseuguette, E.; Mangano, E.; Bisio, C.; Ferrari, M.-C.; Gatti, G. Synthetic Saponite Clays as Additives for Reducing Aging Effects in PIM1 Membranes. *ACS Appl. Polym. Mater.* **2020**, *2*, 3481–3490. [CrossRef]
42. Kebukawa, Y.; Alexander, C.M.O.; Cody, G.D. Comparison of FT-IR Spectra of Bulk and Acid Insoluble Organic Matter in Chondritic Meteorites: An Implication for Missing Carbon during Demineralization. *Meteorit. Planet. Sci.* **2019**, *54*, 1632–1641. [CrossRef]
43. Siriwong, C.; Khansawai, P.; Boonchiangma, S.; Sirisinha, C.; Sae-Oui, P. The Influence of Modified Soybean Oil as Processing Aids in Tire Application. *Polym. Bull.* **2021**, *78*, 3589–3606. [CrossRef]
44. Yuan, H.; Zhang, Y.; Li, Q.; Yan, W.; Zhang, X.; Ouyang, X.; Ouyang, X.; Chen, L.; Liao, B. A Study of Al_2O_3/MgO Composite Films Deposited by FCVA for Thin-Film Encapsulation. *Materials* **2023**, *16*, 1955. [CrossRef]
45. Bartlett, P.N.; Ling-Chung, S.K. Conducting Polymer Gas Sensors Part II: Response of Polypyrrole to Methanol Vapour. *Sens. Actuators* **1989**, *19*, 141–150. [CrossRef]
46. Namsheer, K.; Rout, C.S. Conducting Polymers: A Comprehensive Review on Recent Advances in Synthesis, Properties and Applications. *RSC Adv.* **2021**, *11*, 5659–5697. [CrossRef]
47. Kwak, D.; Lei, Y.; Maric, R. Ammonia Gas Sensors: A Comprehensive Review. *Talanta* **2019**, *204*, 713–730. [CrossRef]
48. Muangrat, W.; Obata, M.; Hashimoto, Y. Enhancement Sensitivity and Selectivity of Ammonium Hydroxide Using Nitrogen-Doped Double-Walled Carbon Nanotubes. *Trends Sci.* **2022**, *19*, 2891. [CrossRef]
49. Ahmadi, S.; Afzalzadeh, R. Few-Layer Graphene Doped with Boron to Enhance Ammonium Hydroxide Vapour Detection at Low Temperature. *Micro Nano Lett.* **2018**, *13*, 363–368. [CrossRef]
50. Liu, K.; Yang, P.; Li, S.; Li, J.; Ding, T.; Xue, G.; Chen, Q.; Feng, G.; Zhou, J. Induced Potential in Porous Carbon Films through Water Vapor Absorption. *Angew. Chem. Int. Ed.* **2016**, *55*, 8003–8007. [CrossRef] [PubMed]
51. Chakraborthy, A.; Nuthalapati, S.; Nag, A.; Afsarimanesh, N.; Alahi, M.E.E.; Altinsoy, M.E. A Critical Review of the Use of Graphene-Based Gas Sensors. *Chemosensors* **2022**, *10*, 355. [CrossRef]
52. Cheng, L.; Ma, S.Y.; Li, X.B.; Luo, J.; Li, W.Q.; Li, F.M.; Mao, Y.Z.; Wang, T.T.; Li, Y.F. Highly Sensitive Acetone Sensors Based on Y-Doped SnO2 Prismatic Hollow Nanofibers Synthesized by Electrospinning. *Sens. Actuators B Chem.* **2014**, *200*, 181–190. [CrossRef]
53. Gong, Y.; Li, H.; Pei, W.; Fan, J.; Umar, A.; Al-Assiri, M.S.; Wang, Y.; Rooij, N.F.d.; Zhou, G. Assembly with Copper(II) Ions and D–π–A Molecules on a Graphene Surface for Ultra-Fast Acetic Acid Sensing at Room Temperature. *RSC Adv.* **2019**, *9*, 30432–30438. [CrossRef] [PubMed]
54. Li, X.B.; Zhang, Q.Q.; Ma, S.Y.; Wan, G.X.; Li, F.M.; Xu, X.L. Microstructure Optimization and Gas Sensing Improvement of ZnO Spherical Structure through Yttrium Doping. *Sens. Actuators B Chem.* **2014**, *195*, 526–533. [CrossRef]
55. Kwon, O.S.; Park, S.J.; Yoon, H.; Jang, J. Highly Sensitive and Selective Chemiresistive Sensors Based on Multidimensional Polypyrrole Nanotubes. *Chem. Commun.* **2012**, *48*, 10526–10528. [CrossRef] [PubMed]
56. Lv, D.; Shen, W.; Chen, W.; Tan, R.; Xu, L.; Song, W. PSS-PANI/PVDF Composite Based Flexible NH3 Sensors with Sub-Ppm Detection at Room Temperature. *Sens. Actuators B Chem.* **2021**, *328*, 129085. [CrossRef]
57. Wu, Q.; Shen, W.; Lv, D.; Chen, W.; Song, W.; Tan, R. An Enhanced Flexible Room Temperature Ammonia Gas Sensor Based on GP-PANI/PVDF Multi-Hierarchical Nanocomposite Film. *Sens. Actuators B Chem.* **2021**, *334*, 129630. [CrossRef]
58. Pagidi, S.; Pasupuleti, K.S.; Reddeppa, M.; Ahn, S.; Kim, Y.; Kim, J.-H.; Kim, M.-D.; Lee, S.H.; Jeon, M.Y. Resistive Type NO_2 Gas Sensing in Polymer-Dispersed Liquid Crystals with Functionalized-Carbon Nanotubes Dopant at Room Temperature. *Sens. Actuators B Chem.* **2022**, *370*, 132482. [CrossRef]

59. Zhao, Q.; Yuan, Z.; Duan, Z.; Jiang, Y.; Li, X.; Li, Z.; Tai, H. An Ingenious Strategy for Improving Humidity Sensing Properties of Multi-Walled Carbon Nanotubes via Poly-L-Lysine Modification. *Sens. Actuators B Chem.* **2019**, *289*, 182–185. [CrossRef]
60. Wang, Z.; Zhu, L.; Wang, J.; Zhuang, R.; Mu, P.; Wang, J.; Yan, W. Advances in Functional Guest Materials for Resistive Gas Sensors. *RSC Adv.* **2022**, *12*, 24614–24632. [CrossRef]